Optimum Receiver Design for OFDM-Based Broadband Transmission—Part II: A Case Study

Michael Speth, Stefan Fechtel, Gunnar Fock, and Heinrich Meyr, *Fellow, IEEE*

***Abstract*—This paper details on the design of OFDM receivers. Special attention is paid to the OFDM-specific receiver functions necessary to demodulate the received signal and deliver soft information to the outer receiver for decoding. In Part I of the paper, the effects of nonideal transmission conditions have been thoroughly analyzed. To show the impact of the synchronization algorithms—which are most critical in OFDM—on system performance and complexity we consider the design of a *complete* receiver consisting of symbol synchronization, carrier/sampling clock synchronization and channel estimation. The performance of the algorithms is analyzed and a qualitative estimate of the resulting complexity is given. This allows to draw conclusions concerning the achievable system performance under realistic complexity assumptions.**

***Index Terms*—OFDM, receiver design, synchronization.**

I. Introduction

DUE TO its many advantages *Orthogonal Frequency Division Multiplexing* (OFDM) is well suited for wireless broadband access systems. A potential drawback of OFDM, however, is its sensitivity to receiver synchronization imperfections. In this context, two questions are of prime interest: 1) How much of the theoretical performance of OFDM can be realized, considering the *complete* inner receiver? 2) Is the complexity of the receivers critically increased by the synchronization algorithms?

Instead of presenting a detailed analysis of isolated algorithms, this paper focuses on the complete system design process considering the European standard DVB-T for digital TV [1]: selection of suitable algorithms, interactions between the receiver tasks, and the tradeoff between receiver complexity and performance.

One focus of the paper is the—often underestimated—task of system acquisition. Fast and reliable system startup requires dedicated algorithms and additional design effort.

II. DVB-T System Parameters

The basic DVB-T modes and parameters important to the inner receiver are: $B = 8$ MHz; $1/T = 64/7$ Mhz; $T_g = 1/4T_u, 1/8T_u, 1/16T_u, 1/32T_u$; Outer code: Reed Solomon RS (204, 188, $t = 8$); Inner code: punctured convolutional code with code rates $r = 1/2, 2/3, 3/4, 5/6, 7/8$; Modulation: 4-, 16-, 64-QAM (optionally hierarchical); 8 k Mode: $N = 8192$, $N_U = 6816$, $T_U = 896\ \mu$s; 2 k Mode: $N = 2048$, $N_U = 1704$, $T_U = 224\ \mu$s.

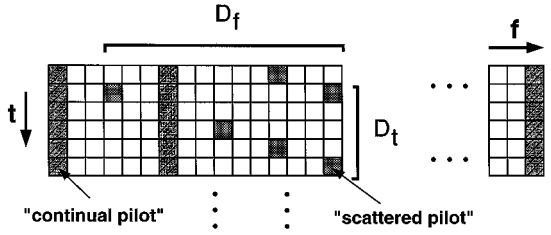

Fig. 1. Arrangement of training data in the DVB-T frame format.

The standard further defines interleaving across subcarriers, the data frame structure, a mechanism for robust signaling of transmission parameters (TPS), and dedicated synchronization symbols $p_{l,k}$ embedded into the OFDM data stream (Fig. 1): 1) *Continual pilot carriers* (45 [2 k mode] and 177 [8 k mode] time-invariant training symbols), and 2) *Scattered pilot cells* (training symbols forming a periodic pattern with period in time $D_t = 4$ and period in frequency $D_f = 12$, see Fig. 1). Both continual and scattered pilot symbols are transmitted at a boosted power level of $E\{|p_{l,k}|^2\} = \beta^2 = 16/9$.

III. Receiver Requirements and Resulting Structure

A. Required SNR

Taking into account the scenarios defined by the standard and the analysis presented in Part I, the following must be determined: 1) The range of SNR γ needed for the required outer receiver performance. 2) The upper bound on the additional noise caused by any transmission imperfection. 3) Bounds on the accuracy of parameter estimation, allowed receiver mobility, and the quality of analog components.

For quasi-error-free (QEF) reception, the projected post-RS BER is $\leq 10^{-11}$, requiring a post-Viterbi BER of $\leq 2 \cdot 10^{-4}$ which is taken for evaluation here. The SNR γ required for QEF reception strongly depends on the transmission channel. The two "Rice" and "Rayleigh" channel models defined in [1] don't represent the critical case of a *single frequency network* (SFN) with its very long artificial echoes. Therefore, we define a simplified SFN model consisting of two discrete paths with comparable gain.

The lowest γ is about 3 dB for QPSK transmission with code rate 1/2. At the other extreme (64-QAM, code rate 7/8), more than 40 dB may be required (SFN channel). A good compromise between bandwidth efficiency and robustness is 64-QAM with

Paper approved by Y. Li, the Editor for Wireless Communications Theory of the IEEE Communications Society. Manuscript received August 23, 1999; revised February 28, 2000 and September 15, 2000.

M. Speth and S. Fechtel are with Infineon Technologies AG D-81541 München, Germany (e-mail: michael.speth@infineon.com; stefan.fechtel@infineon.com).

G. Fock and H. Meyr are with the Institute for Integrated Systems in Signal Processing, University of Aachen, D-52056 Aachen, Germany (e-mail: fock@ert.rwth-aachen.de; meyr@ert.rwth-aachen.de).

Publisher Item Identifier S 0090-6778(01)03152-X.

0090–6778/01$10.00 © 2001 IEEE

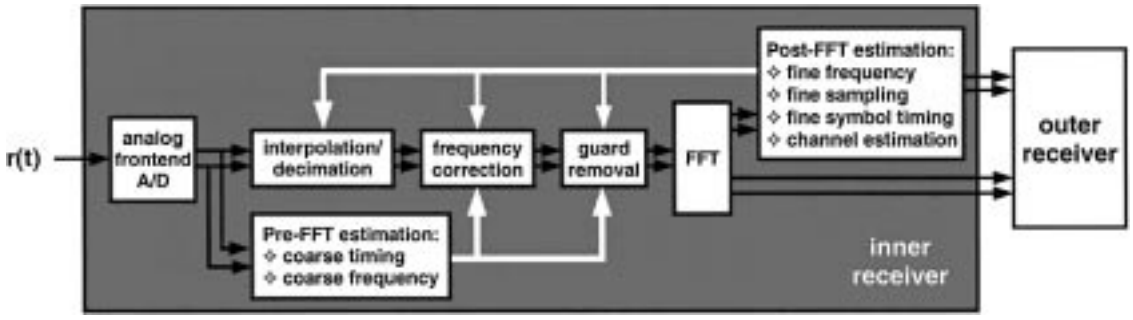

Fig. 2. Structure of a receiver for DVB-T.

code rate 2/3 (mode used in the UK). The required γ in this case ranges between 16.5 dB (AWGN channel) and about 30 dB (SFN channel).

B. Receiver Requirements

Following the principle of synchronized detection [2] the transmission imperfections are estimated in the inner receiver and compensated for. Provided a proper design of the receiver algorithms, the residual imperfections should lead only to a small additional noise component. Given a maximum allowable performance degradation, one can define limits for the allowable errors in the estimated parameters. If, for example, the maximum SNR degradation caused by either receiver component should not exceed 0.1 dB, the analysis in Part I shows that the power of the additional noise contributions must be as small as 16.3 dB below the additive channel noise; the channel estimation gain (as defined in Part I) must also be as high as $G = 16.3$ dB.

Assuming a maximum $\gamma = 30$ dB yields the following receiver requirements:

1) Regarding carrier and sampling frequency, eq. (43) of Part I calls for the maximum relative (local) subcarrier frequency offset $\phi_{\max}$ to satisfy

$$\phi_{\max} < \frac{\sqrt{3}}{\pi}\sqrt{\frac{1}{\gamma}\left(1-\frac{1}{\Delta\gamma}\right)}. \tag{1}$$

Considering $\gamma = 30$ dB and $\Delta\gamma = 0.1$ dB, $\phi_{\max}$ must be smaller than 0.0026 at virtually all times.

2) As for symbol timing, we cannot specify an absolute limit for the offset. Of main concern is the impact of timing errors on the channel estimation. From eq. (33) and (18) of Part I the loss in performance due to the degraded channel estimation can be shown to be given by

$$\Delta\gamma = \frac{G+1}{G(1-\sigma_{\text{add}}^2\gamma)+1} \tag{2}$$

where σ_{add}^2 is the additional variance of the channel estimate caused by a timing error and γ the SNR under consideration. If, for example, channel taps that account for 1% of the total channel energy violate the estimator limits, the impact will be small at $\gamma = 5$ dB. However, at $\gamma = 20$ dB, the resulting loss in performance will be 3 dB which is unacceptable.

C. Receiver Structure

Following the philosophy outlined in [2] the digital and analog parts of the receiver are separated. This is possible by digital timing and sampling clock compensation using interpolation and decimation, and by digital oscillator frequency adjustment using *numerically controlled oscillators* (NCO's).

Most of the receiver structure follows from the kind of available training data. Since there only is post-FFT training data, the receiver features post-FFT oscillator frequency, sampling frequency, and timing estimation as well as channel estimation. However, to provide a fast and reliable acquisition, additional (coarse) pre-FFT algorithms are required. The resulting receiver structure is depicted in Fig. 2.

IV. Receiver Algorithms

A. Channel Estimation

The channel estimation unit must estimate both the channel and any residual phase errors. It thus must be designed to cope with a certain extent of dynamics even in a static channel scenario. The way the scattered pilots are arranged calls for channel estimation via interpolation. In [3] the optimization of the filters for channel estimation is done via a Wiener filter approach. By making use of the (known) pilots, samples $\hat{H}_{l,k} = z_{l,k}/p_{l,k}$ of the CTF are obtained. Final estimates $\tilde{H}_{l,k}$ are generated by interpolation in time and frequency direction. This two-dimensional interpolation problem can be separated into an interpolator in time with transfer function $W_t(f)$ and in frequency with transfer function $W_f(f)$. These interpolators are optimized for an MMSE $\sigma_{\tilde{H}}^2 = E\{|\tilde{H}_{l,k} - H_{l,k}|^2\}$ between channel estimate and actual CTF, taking into account: 1) The **correlation** functions of the CTF in time and frequency, 2) The **variance** of the noise disturbing the samples $\hat{H}_{l,k}$, and 3) The **number** and the **pattern** of the pilots used for estimation.

In order to get an implementationally reasonable solution, the optimization is done off-line, making worst case assumptions for the optimization parameters. The resulting coefficient sets are stored in a ROM and selected according to the mode of operation. For the two interpolation problems the optimization parameters can be identified as follows:

1) Interpolation in Time-Direction:

Correlation: In time direction, the CTF is sampled at time instants $T_t = 4(T_u + T_g)$ apart. For mobile channels the correlation between these samples is determined by the bandwidth of the Jakes spectrum with a maximum doppler frequency f_d and

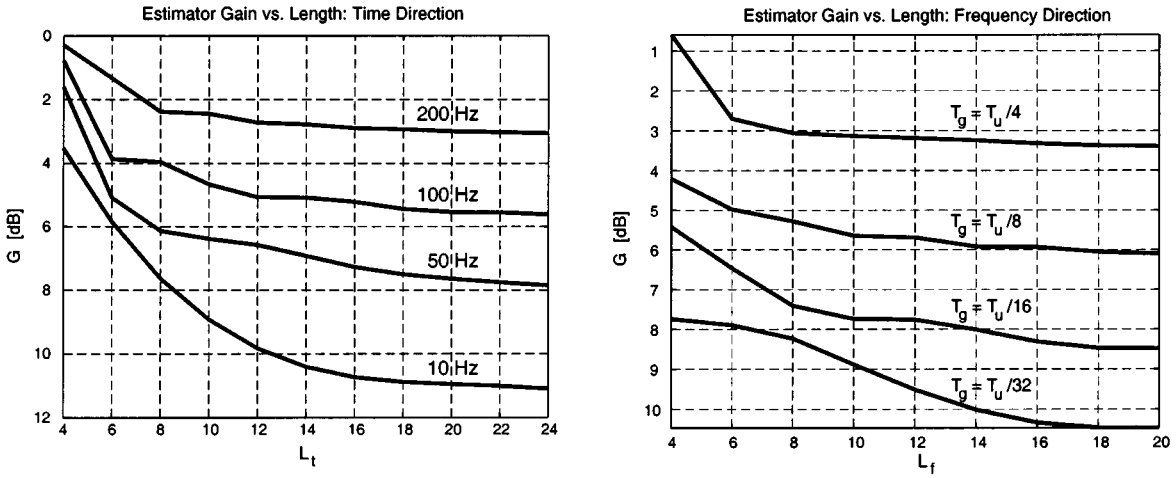

(a) (b)

Fig. 3. Achievable estimator Gain G versus number of coefficients in 2 k mode. Time direction coefficients optimized for $\gamma = 20$ dB. Frequency direction coefficients optimized for $\sigma^2_{\tilde{H}^t} = -22.5$ dB.

the residual local frequency offsets Δf_k remaining after synchronization. The resulting bandwidth is $B_t = 2(f_d + \Delta f_k)$, and the process to be interpolated is oversampled by a factor of

$$r_t = \frac{T_{\max}}{T_t} = \frac{1}{B_t \cdot 4 \cdot (T_u + T_g)} \tag{3}$$

with respect to the Nyquist sampling time $T_{\max}$. Interpolation is only feasible if $r_t > 1$. Since r_t is a measure for the correlation of adjacent samples, the estimation variance $\sigma^2_{\tilde{H}^t} = E\{|\tilde{H}^t_{l,k} - H_{l,k}|^2\}$ decreases as r_t increases.

Variance: Due to the boosted power level, the samples $\hat{H}_{l,k}$ are disturbed by additive Gaussian noise of variance $\sigma^2_{\hat{H}} = 9/16\sigma^2_N$. The performance measure of interest is the estimator gain $G = \sigma^2_N/\sigma^2_{\tilde{H}}$ which thus will be around 2.5 dB even if the estimate is not further improved by interpolation.

Number/Pattern: Best results are achieved if the interpolator coefficients are symmetric with respect to the position to be interpolated. For interpolation in time this means that the same number of causal and noncausal taps is used. For DVB-T this causes a severe complexity problem because noncausal samples can only be acquired by storing all OFDM symbols in between the time instant to be interpolated and the last "noncausal" tap. Since this involves storing four *complete* OFDM symbols for each noncausal tap, the memory required is so large that only linear interpolation is considered in current implementations. However, to show the potential of the DVB-T standard, the theoretical performance as a function of the interpolator length L_t is depicted in Fig. 3(a).

To reach the projected $\Delta\gamma = 0.1$ dB, a total gain of $G = 16.3$ dB must be realized by the estimators. Even in the quasi-static case ($f_d = 10$ Hz) this gain is hardly achieved (gain approaches 16 dB for very large L_t). For the 8 k mode (here results for 2 k mode apply with $4 \cdot f_d$) it is totally out of reach.

2) Interpolation in Frequency Direction:

Correlation: Interpolation in frequency direction is the dual problem of interpolation in time direction: The sampling time corresponds to the frequency spacing $D_f \cdot 1/T_u$ of the CTF samples, the bandwidth B_t to the maximum delay $\tau_{\max}$ of the CIR [3]. In analogy to (3) an oversampling factor for interpolation in frequency direction is derived as

$$r_f = \frac{T_u}{D_f}\frac{1}{\tau_{\max}}. \tag{4}$$

The given frequency spacing allows interpolation only for channels with $\tau_{\max} \leq T_u/12$. If interpolation in time precedes interpolation in frequency direction, the resulting effective $D'_f = 3$ allows interpolation even for the largest guard interval $T_g = T_u/4$. Since r_f increases as $\tau_{\max}$ decreases the quality of the interpolation can be improved for short CIR's compared to long CIR's if this *a-priori* information is taken into account in the estimator. Since T_g is known it can be used as an upper bound for $\tau_{\max}$. Note that matching the interpolator transfer function too closely to the guard interval bears the risk of making the system very vulnerable to timing errors or channel components outside the guard interval.

Variance: Since interpolation in time precedes interpolation in frequency, the variance of the noise process to be considered is the $\sigma^2_{\tilde{H}^t}$ after interpolation in time direction.

Number/Pattern: In frequency direction symmetric interpolation can be applied. Fig. 3(b) shows the achievable gain versus the interpolator length L_f. (Note the initial gain of 2.5 dB due to the boosted pilots.)

As the results indicate, matching the estimators to the presumed channel length yields a significant performance gain. But even for the smallest guard interval interpolation in frequency alone will not be sufficient to reach the design goal of $G = 16.3$ dB. Optimizing the estimators with respect to the SNR yields no significant additional gain. Hence fixed coefficients matched to the highest expected SNR can be applied.

As for implementation complexity, the analysis above suggests the following choices:

- For interpolation in time direction, a linear interpolator is used. The complexity is dominated by the memory needed to provide for the noncausal tap; this entails the storage of 3 additional OFDM symbols (3*6816 QAM symbols).

- For interpolation in frequency direction, 12 coefficients are used, resulting in 24 MAC's per QAM symbol. Considering all possible modes of operation and the fact that additional coefficient sets must be provided for the spectrum edges, a total of 128 coefficient sets is necessary.

B. Coarse Timing Synchronization

As derived in Part I and shown in Section II B of this part, the proper selection of the FFT window has a major performance impact on all post FFT algorithms. Therefore, it is most desirable to achieve good timing synchronization early in the acquisition. Since there is no pre FFT training data, *nondata-aided* (NDA) algorithms using pre FFT data are used. The task would still be easy if it wasn't for the impairments imposed by the (unknown) frequency offset and channel. Due to these impairments the only information that can be used is the knowledge of the guard interval structure. Since the guard interval is the repetition of a section of normal data, a coarse estimate can be obtained by detecting this repetition.

Numerous approaches to this task are known. In [4] the standard approach of a simple correlation metric is compared to MMSE and ML based algorithms. Under AWGN and moderately dispersive conditions the more sophisticated algorithms (MMSE and ML) show considerable performance gains. But in ISI channels (in particular SFN) there is always a nonnegligible probability of failure even for the most complex algorithms. A mechanism for detection of such failures has to be implemented that forces the timing synchronization to be repeated until a sufficient accuracy is achieved.

The true design goal for coarse timing synchronization is not to achieve the highest possible accuracy, but to meet the requirements of the following algorithms with a minimum number of trials. This reasoning leads to the selection of the maximum correlation metric [eq.(5)] which has minimal implementation cost and sufficiently low probability of failure for typical scenarios:

$$\hat{n}_{\varepsilon} = \arg\max_{n_{tr}} \left| \sum_{i=n_{tr}}^{n_{tr}+N_G-1} r^*(i) r(i+N) \right|. \tag{5}$$

Whereas (5) is tolerable to large frequency offsets, the potentially large sampling frequency deviations ζ during acquisition must be considered. Typically timing deviations as large as $1/T$ between the two samples (T_U apart) used for correlation have to be taken into account. A possible solution to this problem is to implement three correlators with delays of $N-1$, N and $N+1$. The outputs of all three correlators are then fed into separate gliding windows that calculate the sum $\sum_{i=k}^{k+N_G-1}$. A single metric is derived from these three gliding window outputs by taking the maximum of the three output values. The actual timing estimate is then calculated by a maximum search over $N+N_G$ metric values.

As far as the hardware complexity is concerned, the conjugate multiplication is the operation with the highest complexity. However, the necessary wordlength can be reduced significantly so that complexity is dominated by the delay line storing the samples of a complete OFDM symbol.

C. Carrier and Sampling-Clock Synchronization

In this section, we consider the carrier frequency offset Δf and relative sampling frequency offset $\zeta = \Delta T/T = -(\Delta f_s/f_s)$ (signal models see Part I), with ΔT and Δf_s the sampling duration offset and sampling frequency offset, respectively. We distinguish between an "integer" carrier frequency offset Δf_I, being a multiple of the subcarrier spacing $1/T_u$, and a "fractional" carrier frequency offset Δf_F being responsible for subcarrier misalignment and thus ICI:

$$\begin{aligned} \Delta f &= \Delta f_I + \Delta f_F = (n_I + \Delta f'_F)(1/T_u) \\ \Delta f' &= \Delta f \cdot T_u = n_I + \Delta f'_F. \end{aligned} \tag{6}$$

1) Frequency Synchronization Strategy: As outlined in the last section of Part I, the objective of frequency sync is to establish subcarrier orthogonality as fast and accurately as possible (acquisition) and then maintain orthogonality as well as possible at all times during online reception (tracking). However, a (pre- or post-FFT) OFDM frequency acquisition algorithm *alone* cannot, in general, be both fast and sufficiently accurate, because

- pre-FFT algorithms allow fast acquisition of the *fractional* carrier frequency $\Delta f'_F$ but no or very slow acquisition of n_I
- post-FFT algorithms allow fast acquisition of the *integer* carrier frequency n_I but, due to lack of orthogonality, acquisition of $\Delta f'_F$ is either quite complex or very slow.

Both fast and accurate acquisition can be attained by adopting a multi-stage synchronization strategy, in particular, two one-shot acquisition stages (one pre-FFT and the other post-FFT), followed by tracking. In DVB-T, the data format provides for post-FFT training (continual and/or scattered pilots) but not for pre-FFT training. Hence, pre-FFT NDA (nondata-aided) and post-FFT DA (data-aided) acquisition and tracking algorithms are suitable. This leads to the following frequency sync architecture in DVB-T reception:

1) pre-FFT NDA acquisition $\longrightarrow \Delta f'_F$
2) post-FFT DA acquisition $\longrightarrow n_I$
3) post-FFT DA tracking $\longrightarrow \Delta f'_F, \zeta$.

The control loops of the three-stage synchronization subsystem operate on a per-OFDM-symbol basis. When the carrier frequency detector (CFD) has generated an estimate of $\Delta f'_F$ and/or n_I, carrier frequency correction is effectuate by adjusting the I/Q mixer NCO shortly before the beginning of the next (pre-FFT) OFDM symbol. Likewise, when the sampling frequency detector (SFD) has generated an estimate of ζ, sampling frequency correction is done by adjusting the resampling NCO shortly before the beginning of the next (pre-FFT) OFDM symbol.

2) Pre-FFT Carrier Frequency Acquisition: Like coarse timing sync, DVB-T pre-FFT frequency acquisition is based on guard interval correlation. Disregarding ISI and sampling frequency error for the moment, the received samples $r_{l,n} = r_{n'}$ [eq. (35) of Part I] show the same property except for a phase rotation between guard and tail segments being proportional

to the *fractional* carrier frequency offset $\Delta f'_F$. Guard interval correlation samples thus become

$$\begin{aligned} x_{n'} &= r_{n'} \cdot r^*_{n'-N} \\ &\propto e^{j2\pi\Delta f'_F} + noise. \end{aligned} \tag{7}$$

Given these samples $x_{n'}$ and the coarse timing window estimate $\hat{n}'$, the ML frequency estimate [5] becomes

$$\Delta\hat{f}'_F = \frac{1}{2\pi} \cdot \arg\left[y_{\hat{n}'} \sum_{i=\hat{n}'-(L-1)}^{\hat{n}'} x_i \right]. \tag{8}$$

An analysis of the estimation performance [6] shows that estimation accuracy is largely dominated by self-noise. However, the accuracy in the order of 1–2 percent is perfectly adequate for the first sync stage.

3) Post-FFT Carrier Frequency Acquisition: In the presence of large offsets $\Delta f' = n_I + \Delta f'_F$, the post-FFT signal model (37) of Part I can be cast into the form

$$\begin{aligned} z_{l,k} = &\left(e^{j\pi\phi'_{k'}} \cdot e^{j2\pi((lN_s+N_g)/N)(n_I+\phi'_{k'})} \right) \cdot \alpha(\phi'_{k'}) \\ &\cdot H_{k'} a_{l,k'} + n_{\Omega;l,k} + n_{l,k} \end{aligned} \tag{9}$$

with

$$\begin{aligned} \phi'_{k'} &= \Delta f'_F + \zeta \cdot k' \\ k' &= k - n_I. \end{aligned} \tag{10}$$

Thanks to pre-FFT acquisition, the *residual* fractional offset $\Delta f'_F$ is small so that stage-2 estimation ICI noise $n_{\Omega;l,k}$ [power given by (41) of Part I] is also small. In essence, the k'th transmitted subcarrier shows up at FFT output bin with index $k = k' + n_I$. The spectral shift n_I (subcarrier spacings) must now be detected using the C continual pilots $c_{k'}$ located at certain subcarrier positions $k' \in \mathcal{C}$. The set of transmitted pilots $c_{k'} (k' \in \mathcal{C})$ show up at the set of FFT output bins $k \in \mathcal{C} + n_I$. The translation n_I can be found by exploiting that the transmitted CP's are both boosted in power (factor β^2) and modulated by time-invariant symbols. Correlating FFT output samples of two consecutive OFDM symbols $l-1$, l then yields

$$\begin{aligned} x_k &= z_{l,k} \cdot z^*_{l-1,k} \\ &= e^{j2\pi(N_s/N)(n_I+\phi'_{k'})} \cdot \alpha^2(\phi'_{k'}) \cdot |H_{k'}|^2 \\ &\quad \cdot \left\{ \begin{array}{cc} \beta^2\sigma_a^2 & k \in \mathcal{C} + n_I \\ (b_{l,k'} b^*_{l-1,k'}) & k \in \mathcal{B} + n_I \\ 0 & \text{otherwise} \end{array} \right\} + noise \end{aligned} \tag{11}$$

with $k' \in \mathcal{B}$ the set of transmitted non-CP samples $b_{l,k'}$ (TPS, SP, QAM) appearing random at this stage.

Similar to the stage-1 ML algorithm, the C correlation samples x_k pertaining to a particular set $k \in \mathcal{C} + m$ are accumulated, yielding a phasor y_m. This is done for all $m \in \mathcal{I}$, where the search range $\mathcal{I}$ is typically given by $[-n_{I,\max}, n_{I,\max}]$. The maximum absolute value $|y_m|$ then yields the integer carrier frequency estimate $\hat{n}_I$:

$$\hat{n}_I = \arg\max_{m \in \mathcal{I}} \left| \sum_{k \in \mathcal{C}+m} x_k \right|. \tag{12}$$

Considering small (residual) offsets $\Delta f'_F$ and ζ, a small-signal statistical model of phasor y_m [6] shows that, for relevant SNR's of 5 dB and above, the probability of false detection ($\hat{n}_I \neq n_I$) is very small.

4) Post-FFT Carrier and Sampling Frequency Tracking: In tracking mode, only a small residual carrier frequency offset $\Delta f' = \Delta f'_F$ remains. The sampling frequency offset ζ may initially be larger but within the tracking convergence range; in steady-state tracking, both $\Delta f'$ and ζ are small.

The carrier (CFD) and sampling (SFD) frequency detectors in post-FFT DA tracking are again based on post-FFT temporal correlation:

$$\begin{aligned} x_{l,k} &= z_{l,k} \cdot z^*_{l-1,k} \\ &= e^{j2\pi(1+N_g/N)\phi_k} \cdot \alpha^2(\phi_k) \cdot |H_k|^2 \cdot \beta^2\sigma_a^2 + noise \end{aligned} \tag{13}$$

[see (39) of Part I] with $\phi_k = \Delta f' + \zeta \cdot k$ the subcarrier symbol rotation.

The symbol rotation trajectory ϕ_k, $k = -(K-1)/2, \cdots, +(K-1)/2$ (Fig. 6 of Part I) suggests a simple CFD/SFD algorithm. Let $\mathcal{C}_1$ denote the set of C_1 CP indices in the *left* half $k \in [-(K-1)/2, 0)$ and $\mathcal{C}_2$ the set of C_2 CP indices in the *right* half $k \in (0, +(K-1)/2]$ of the OFDM spectrum. The CP's are distributed equally in both halves of the spectrum ($C_1 = C_2 = (C-1)/2$), and accumulation of $x_{l,k}$ in two parts leads to the CFD/SFD algorithm

$$\begin{aligned} \Delta\hat{f}'_l &= \frac{1}{2\pi(1+N_g/N)} \cdot \frac{1}{2} \cdot (\varphi_{2,l} + \varphi_{1,l}) \\ \hat{\zeta} &= \frac{1}{2\pi(1+N_g/N)} \cdot \frac{1}{K/2} \cdot (\varphi_{2,l} - \varphi_{1,l}) \\ \varphi_{(1|2),l} &= \arg\left[y_{(1|2),l} = \sum_{k \in \mathcal{C}_{(1|2)}} x_{l,k} \right] \end{aligned} \tag{14}$$

[$(1|2)$ denoting 1 for left and 2 for right half].

The (one-shot) CFD/SFD estimates $\Delta\hat{f}'_l, \hat{\zeta}$ are then post-processed by their own PI (proportional-integral) tracking loops.

The choice of loop parameters $K_{P,f}$ and $K_{P,\zeta}$ for the carrier and sampling tracking loops, respectively, determines the amount of residual ICI and thus the SNR loss $\Delta\gamma$. Using eq. (1) and considering a safety margin of 6 times the error standard deviation σ_ϕ, the carrier frequency loop parameter $K_{P,f}$ must satisfy

$$K_{P,f} \leq \frac{1}{6} \left(1 + \frac{N_g}{N} \right)^2 \beta^2 C \left(1 - \frac{1}{\Delta\gamma_{\max}} \right). \tag{15}$$

In DVB-T steady-state reception (quasi-static channel), a very small maximum SNR loss of $\Delta\gamma = 0.02$ dB at all SNR γ results for the choice $K_{P,f} = (1/16|1/4)$ and $K_{P,\zeta} = (1/64|1/16)$ in (2 k | 8 k) mode.

Fig. 4 shows an example of carrier frequency tracking convergence and steady-state behavior for DVB-T 2 k mode; one-shot CFD offset estimates (SNR 10 dB) are also displayed for reference. Starting from a (relatively large) initial offset 0.1, convergence is achieved after less than 50 symbols, and the steady-state error remains small even at low SNR.

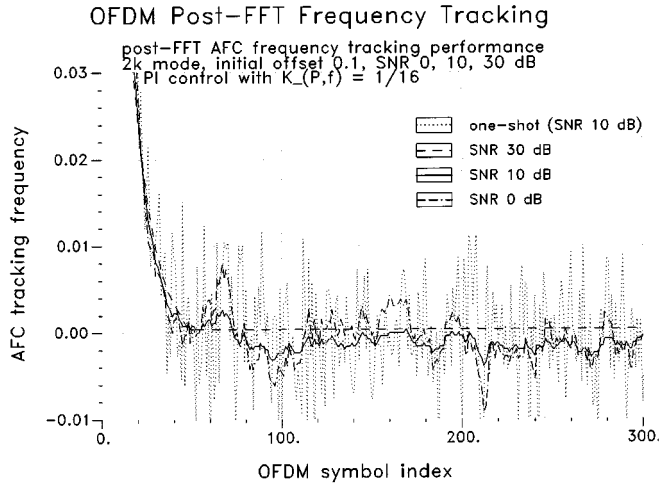

Fig. 4. Post-FFT carrier frequency tracking performance.

The complexity of frequency synchronization is easily determined from the algorithms presented above. The preprocessing part (continual pilot sample correlation) is dominant, while the postprocessing tasks (generating estimates and control values) are performed at a relatively low rate and can thus be mapped onto area-efficient serial architectures.

D. Fine-Timing Synchronization

Since the mechanism used for coarse timing synchronization is not able to provide the accuracy needed, a different effect must be exploited to further refine the initial estimate. The algorithm considered here requires that sampling and carrier frequency are already synchronized. Hence fine timing will be the last task in the acquisition process.

In [7] the following synchronization metric based on the maximum likelihood principle has been derived:

$$\Lambda_T(n_{tr}) = \sum_{k\in P} |z_{l,k}(n_{tr}) - p_{l,k}\cdot \tilde{H}_{l,k}(n_{tr})|^2 \qquad (16)$$

where P is the set of subcarriers bearing scattered pilots and $H_{l,k}(n_{tr})$ is the transfer function of the *effective channel* as introduced in Part I. In order to support all modes of operation the scattered pilots of four consecutive OFDM symbols are used. All variables are functions of n_{tr} since they change as the current FFT window position n_{tr} changes. Minimizing (16) with respect to the trial window position n_{tr} yields an estimated $\tilde{n}_\varepsilon$ for the number of samples the window position has to be corrected. If $W_f(f)$ is matched to the guard interval as is the case here, (16) can be further simplified to yield

$$\Lambda_H(n_{tr}) = \sum_{k\in P} |\tilde{H}_{l,k}(n_{tr})|^2. \qquad (17)$$

Now *maximizing* $\Lambda_H(n_{tr})$ will yield the estimate.While easy to implement (the channel estimation unit is needed anyway), both metrics suffer from a major drawback: the window position is a *pre-FFT* parameter whereas the metric is generated *after* the FFT. This results in an intolerably long acquisition time. An alternative is to generate a fixed estimate of the CIR and to test the trial positions by using a gliding window. Good results are achieved with a simple rectangular window of length T_g.

1) Properties of the Estimated CIR: An estimate for the CIR can be obtained by applying an IFFT to the CTF samples $\hat{H}_{l,k}$ that are used for channel estimation. Using the scattered pilots of four consecutive OFDM symbols a total of $K_{\max}/3+1$ samples are available. To provide a sufficiently accurate estimate a zero padded IFFT of size $N/2$ must be used. The resulting estimated CIR is sampled with a resolution of

$$T' = T\frac{N}{3N_{est}} = 2/3T \qquad (18)$$

and periodic with period $T_P = T_u/3$. Due to this periodicity the estimate is ambiguous. Fig. 5 depicts the situation for the largest guard interval ($N_g = 512$ in 2 k mode). The CIR can be as long as the guard interval which is equivalent to the first $N'_g = 3/2N_g$ samples of the estimate. If a large timing offset remains after coarse timing, CIR components of a preceding period can be shifted into the evaluation window, leading to an erroneous result. To avoid an ambiguous CIR estimate the error after coarse timing must satisfy

$$n_{\varepsilon,\max} = \tfrac{1}{6}(N - 3N_G). \qquad (19)$$

The case depicted in Fig. 5 yields a small $n_{\varepsilon,\max} = 85$. If this limit is violated, advanced post-processing must be applied to resolve the resulting ambiguity.

There are a lot of possibilities to derive the timing information from the estimated CIR (i.e., detecting the "beginning" and "end" of the CIR). However, the original metric (17) indicates the optimum method: maximize the energy of the CIR estimate within a sliding window of size N'_g for all trial positions within the interval $[-(3/2)n_{\varepsilon,\max}, +(3/2)n_{\varepsilon,\max}]$.

If the CIR is smaller than the guard interval there is no single "correct" timing position. Consequently consecutive estimates (i.e., in tracking mode) will not necessarily yield the same position. This raises the question of how the window position can be corrected.

2) Timing Error Correction: Fine timing synchronization will have two modes of operation: 1) *Acquisition*: correction of the remaining offset after coarse timing correction. 2) *Tracking*: correction of small changes (caused by the drift of the sampling clock) during normal operation. Whereas the first case is not critical (during acquisition no data must be detected), in tracking mode the impact of the window position on the effective channel $h_\varepsilon(\tau)$ must be kept in mind. The CTF of the effective channel is related to the CTF of the actual channel via the relation:

$$H^{\varepsilon}_{l,k} = H_{l,k}\cdot e^{j2\pi(k/N)n_\varepsilon}. \qquad (20)$$

Consequently, a change in timing position by n_ε causes strong phase rotations. Since the channel estimator possesses a memory, the resulting shifts in phase have to be compensated. A simple method that avoids this compensation is to make use of the window drift caused by a small deliberate sampling frequency offset. If the sampling clock is slightly detuned, small timing offsets can be corrected. To achieve this the sampling frequency loop filter is modified by a correction (detuning) value ζ_d (see above). The correcting offset ζ_d will bias the estimator: Consequently even if its absolute value is much smaller

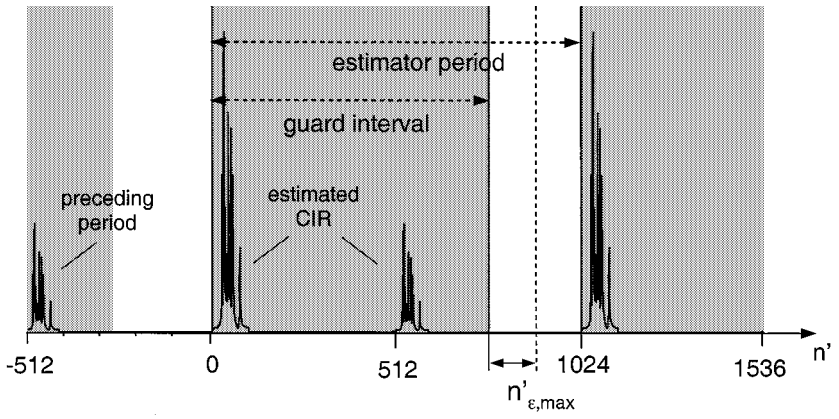

Fig. 5. Ambiguity due to periodicity of CIR estimate. 2 k mode, $N_g = 512$.

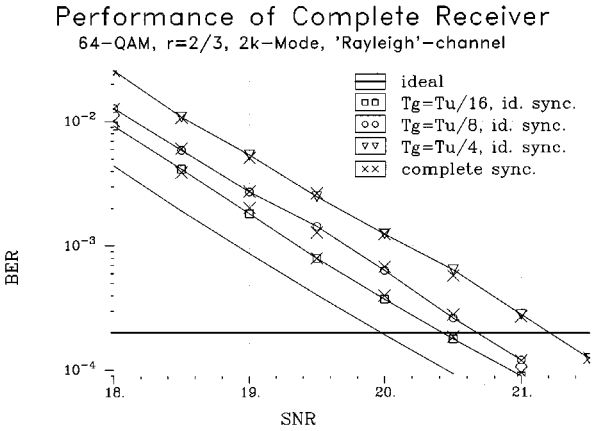

Fig. 6. Performance of DVB-T receiver. DVB-T 2 k mode, "Rayleigh" channel, 64-QAM rate $= 2/3$.

than the variance of the estimator, the accumulated (desired) error slowly adapts the window position. Using a fixed ζ_f that is considerably smaller than the allowable residual offset of the sampling clock synchronization loop proves a good choice. In this case the timing error correction unit simplifies to the rule:

$$\zeta_d = \begin{cases} -|\zeta_f|, & \text{for } \hat{n}_\varepsilon \leq 0 \\ +|\zeta_f|, & \text{for } \hat{n}_\varepsilon > 0. \end{cases} \tag{21}$$

The complexity of this unit is dominated by the 4 k IFFT needed for CIR estimation. Since the timing changes slowly, speed is not important. It may suffice to implement one FFT-butterfly so that main concern again is the memory needed.

V. Receiver Performance and Complexity

Again we consider the case of 64 QAM with code-rate 2/3. Fig. 6 shows the receiver performance for the "Rayleigh" channel with different T_g (and different corresponding channel estimators). The degradation $\Delta\gamma$ ranges from 1.4 dB for the largest T_g to about 0.5 dB for the smallest. Although the (unrealistic) goal of a 0.1-dB penalty is not met, the result is surprisingly good if compared to systems like GSM. This is the result of the system-inherent trade-off between training overhead, projected receiver complexity and performance made in this particular standard. The price—in terms of complexity—of further improvement by more sophisticated channel estimation is high, in particular for the 8-k mode.

A further measure of interest is the additional degradation caused by the synchronization algorithms. Fig. 6 includes the receiver performance with the complete synchronization chain developed in the previous sections. The loop parameters are chosen according to Section IV-C, with $\zeta_d = 10^{-6}$. Synchronization is seen to have almost no influence on the performance. Taking into account the well-known vulnerability of OFDM to synchronization errors, this result is remarkable.

As far as complexity is concerned, the dominating component is the 8 k-FFT. Second largest component is the channel estimator with its symbol memory. The complexity of synchronization algorithms turns out to be rather moderate, fine timing synchronization being the most complex of the synchronization algorithms. Nevertheless, if SFN scenarios are to be supported, this effort must be spent.

VI. Discussion and Conclusion

In this paper we have considered the systematic design of inner receiver algorithms for OFDM-based transmission systems. Following the analysis in Part I, we have determined the requirements on the receiver components. Taking into account the frame structure of the DVB-T scenario, we have derived algorithms with close-to-optimum performance while providing robust and fast acquisition.

Against common belief, the performance of the receiver is not limited by the achievable quality of synchronization but rather by channel estimation, more specifically, its implementation complexity. The quality of channel estimation is determined by the (assumptions on) the maximum dispersion of the channel. The resulting performance is between 0.5 dB for the smallest, and 1.5 dB for the largest guard interval.

The complexity of the receiver is dominated by the 8 k FFT. In comparison, the complexity of synchronization algorithms is small. The second largest component is the channel estimation. Allowing significantly more complexity for this component the receiver performance could be further improved.

References

[1] ETSI, "Digital broadcasting systems for television, sound and data services: DRAFT pr ETS 300 744,", Mar. 1997.

[2] H. Meyr, M. Moeneclaey, and S. Fechtel, *Digital Communication Receivers: Synchronization and Channel Estimation Algorithms*. New York: Wiley, 1997.
[3] F. Classen, M. Speth, and H. Meyr, "Channel estimation units for an OFDM system suitable for mobile communications," in *Mobile Kommunikation: ITG-Fachbericht*. München, Germany: ITG, VDE-Verlag, Berlin Offenbach, Sept. 1995.
[4] S. Müller-Weinfurtner, "On the optimality of metrics for coarse frame synchronization in OFDM: A comparison," in *Proc. IEEE Int. Symp. on Personal, Indoor, and Mobile Radio Communications*, Boston, MA, Sept. 1998, pp. 533–537.
[5] T. Schmidl and D. Cox, "Robust frequency and timing synchronization for OFDM," *IEEE Trans. Commun.*, vol. 45, Dec. 1997.
[6] S. Fechtel, "Pre- and post-FFT frequency synchronization for DVB-T OFDM reception," *IEEE Trans. Commun.*, submitted for publication.
[7] M. Speth, F. Classen, and H. Meyr, "Frame synchronization of OFDM systems in frequency selective fading channels," in *Proc. IEEE Int. Conf. on Vehicular Technology*, 1997.